Check for updates

Advanced Optical Materials

ADVANCED OPTICAL MATERIALS
www.advopticalmat.de

RESEARCH ARTICLE

Ultrafast SLM-Enabled Femtosecond Line-Focus Writing of Angle-Programmable Tilted Fiber Bragg Gratings

Deng Pan[1,4] | Yihang Yin[1] | Hai Hu[1] | Zhijuan Fuyang[1] | Chenchu Zhang[2] | Hui Wang[1] | Shenglai Zhen[1] | Yanlei Hu[3] | Jiawen Li[3] | Zhaoxin Lao[2] | Zhiqiang Wang[1] | Benli Yu[1] | Dong Wu[3]

[1]State Key Laboratory of Opto-Electronic Information Acquisition and Protection Technology, Anhui University, Hefei, China | [2]Anhui Province Key Lab of Aerospace Structural Parts Forming Technology and Equipment, School of Mechanical Engineering, School of Instrument Science and Opto-Electronics Engineering, Hefei University of Technology, Hefei, China | [3]Department of Precision Machinery and Precision Instrumentation, University of Science and Technology of China, Hefei, China | [4]Intelligent Interconnected Systems Laboratory of Anhui Province, Hefei University of Technology, Hefei, China

Correspondence: Chenchu Zhang (hfutzcc@hfut.edu.cn) | Shenglai Zhen (zhiqiangwang@ahu.edu.cn) | Zhiqiang Wang (zhiqiangwang@ahu.edu.cn)

Received: 12 June 2026 | **Revised:** 13 October 2026 | **Accepted:** 2 November 2026

Keywords: femtosecond line-focus inscription | mode-locked fiber laser | refractive index sensing | Tilted fiber Bragg gratings

ABSTRACT

Tilted fiber Bragg gratings (TFBGs) are important in-fiber components for sensing, polarization control, and ultrafast photonics, yet their scalable fabrication remains limited by the trade-off between writing speed, angular flexibility, and spectral quality. Here we report an SLM-enabled femtosecond line-focus inscription strategy for ultrafast, angle-programmable fabrication of TFBGs. By loading a cylindrical-lens phase hologram onto the spatial light modulator, a high-aspect-ratio femtosecond focal field is generated inside the fiber core, whose orientation can be dynamically controlled to fabricate TFBGs with tilt angles from 0° to 45° without replacing optical components or phase masks. The line-focus geometry converts conventional serial point writing into continuous high-speed inscription, reducing the fabrication time of a typical TFBG to 0.56 s while maintaining strong cladding-mode resonances. Low-tilt TFBGs exhibit refractive-index sensitivity of 410.7 nm/RIU and enable cascaded moisture sensing and plant water-status monitoring. High-tilt TFBGs function as polarization-dependent in-fiber elements for nonlinear-polarization-rotation mode locking, producing stable 808 fs pulses with a 77.8 dB RF signal-to-noise ratio. This work establishes programmable femtosecond line-focus inscription as a scalable platform for application-specific TFBGs in distributed sensing and ultrafast fiber photonics.

1 | Introduction

Optical fiber sensing provides an important approach to biomedical monitoring and wearable health assessment. A wearable photonic smart wristband based on an all-polymer sensing unit has demonstrated cardiorespiratory function assessment and biometric identification [1]. These advances motivate the development of functional fiber-optic sensing devices and flexible fabrication methods. Tilted fiber Bragg gratings (TFBGs) constitute a powerful in-fiber platform for optical sensing, polarization control, and fiber-integrated photonic devices. In contrast to conventional fiber Bragg gratings, whose grating planes are perpendicular to the fiber axis, TFBGs possess refractive-index modulation planes tilted with respect to the propagation direction. This geometric asymmetry enables controlled coupling from the forward-propagating core mode to backward-propagating core, cladding, or radiation modes, giving rise to a rich set of angle-dependent optical responses [2]. In the low-tilt regime, efficient coupling from the core mode to backward-propagating cladding modes produces dense cladding-mode resonances that are highly sensitive to external perturbations [3], enabling refractive-index, temperature, and pressure sensing [4–8]. At

All rights reserved, including rights for text and data mining and training of artificial intelligence technologies or similar technologies.
© 2026 Wiley-VCH GmbH

larger tilt angles, the broken cylindrical symmetry gives rise to strong polarization-dependent coupling [9], opening opportunities for polarization modulators, polarization-sensitive sensors, laser communication components, and fiber-laser devices [10, 11]. These angle-dependent functionalities make broad and precise tilt-angle programmability a key requirement for practical TFBG fabrication across diverse application scenarios.

Despite their promise, the broader deployment of TFBGs remains constrained by fabrication limitations. Conventional femtosecond point-by-point inscription offers flexible 3D refractive-index modification, but the serial nature of the writing process intrinsically limits throughput [12], especially when long gratings or cascaded grating arrays are required [13, 14]. Interferometric and phase-mask-based approaches can improve fabrication efficiency [15, 16], but they often rely on fixed optical configurations or application-specific masks [17, 18], which restrict rapid tuning of the grating period and tilt angle [19].Slit-based beam shaping offers an alternative approach to generating elongated focal fields [19], although the associated beam blocking can reduce energy utilization and affect focal-field quality [20, 21]. Our experimental comparison shows that SLM-based shaping provides higher useful optical power utilization than the tested slit configuration. As a result, existing methods usually require a trade-off among fabrication speed, structural controllability, energy efficiency, and spectral performance. A general fabrication strategy that simultaneously enables high-speed inscription, programmable tilt-angle control, and high-quality TFBG spectra remains highly desirable.

Femtosecond-laser inscription offers an attractive route because it can induce permanent refractive-index modification within the fiber through highly localized nonlinear interaction [23, 24], enabling flexible and thermally robust grating fabrication. However, to fully exploit these advantages for rapid TFBG fabrication, the femtosecond focal field must be engineered beyond a conventional diffraction-limited point focus. A line-shaped focal field can in principle transform the inscription process from serial point-by-point writing into a quasi-parallel line-by-line process, thereby greatly simplifying the motion trajectory and increasing the fabrication speed. The key challenge is to generate such a line-shaped femtosecond field with high energy utilization, controllable orientation, and stable focal-field quality.

Here we report a spatial-light-modulator-enabled (SLM-enabled) femtosecond-laser inscription strategy for ultrafast and angle-programmable fabrication of TFBGs. By loading a programmable cylindrical-lens phase hologram onto the SLM, the incident femtosecond laser is transformed into a high-aspect-ratio line-shaped focal field inside the fiber core. The orientation of the line focus can be continuously controlled by rotating the phase hologram, allowing TFBGs with tilt angles from 0° to 45° to be fabricated without replacing optical components or phase masks. Because each femtosecond pulse contributes to a line-shaped modification region, high-quality TFBGs can be written through a simple continuous translation of the fiber, with a typical inscription time of only 0.56 s per grating.

Using this programmable line-focus inscription platform, we systematically investigate the effects of grating length, tilt angle, pulse energy, and grating period on the spectral characteristics of TFBGs. Low-tilt TFBGs exhibit strong cladding-mode resonances and high refractive-index sensitivity, enabling cascaded multi-point moisture sensing and plant water-status monitoring. High-tilt TFBGs show polarization-dependent transmission suitable for all-fiber nonlinear-polarization-rotation mode locking, producing stable sub-picosecond pulses with a signal-to-noise ratio of 77.8 dB. These results establish SLM-based femtosecond line-focus inscription as a flexible, efficient, and scalable platform for fabricating application-specific TFBGs, opening new opportunities in distributed fiber sensing, polarization-selective photonics, and ultrafast fiber lasers.

2 | Results

2.1 | Programmable Line-Shaped Femtosecond Field for TFBG Inscription

To overcome the throughput limitation of conventional point-by-point TFBG inscription, we developed a programmable femtosecond line-focus writing system based on SLM-mediated wavefront shaping (Figure 1a). The central concept is to replace the conventional diffraction-limited focal spot with a high-aspect-ratio line-shaped focal field whose orientation can be dynamically controlled. In this configuration, the SLM is loaded with a cylindrical-lens phase hologram to impose an anisotropic wavefront curvature on the incident femtosecond beam. Based on our previous study [25], after focusing through a high-numerical-aperture oil-immersion objective, the modulated beam forms an elongated focal field at the focal plane. Continuous translation of the fiber then converts this line-shaped optical field into a tilted refractive-index modulation pattern, enabling rapid inscription of TFBGs.

A frequency-doubled femtosecond laser amplifier operating at 517 nm with a pulse duration of 290 fs and a repetition rate of 200 kHz was used as the inscription source. The pulse energy was adjusted by a half-wave plate and a Glan–Taylor prism. After beam expansion, the Gaussian beam was reflected by the SLM and focused into the core region of a stripped single-mode fiber through a 60× oil-immersion objective with a numerical aperture of 1.35. The fiber was mounted on a 3D translation stage, allowing the focal field to be accurately positioned at the fiber core and translated along the designed writing direction.

To verify the field-shaping mechanism, numerical simulations were performed for the SLM-modulated femtosecond beam. When the cylindrical-lens phase (focal length of 1250 mm [26, 27]) was applied, the focused optical field evolved from a Gaussian-like input beam (Figure 1b) into a well-defined line-shaped focal distribution with a high aspect ratio. Rotating the cylindrical-lens phase hologram on the SLM resulted in a corresponding rotation of the focal line, providing a direct and programmable means of controlling the TFBG tilt angle (Figure 1c). The grating tilt angle is defined relative to the direction perpendicular to the fiber axis; ideally, 0° corresponds to grating traces perpendicular to the fiber axis. The nominal 0° sample exhibited a mean measured tilt of 0.842° with a sample standard deviation of 0.214° across ten traces in the microscope imaging plane, and therefore represents a near-zero-tilt structure. CCD observations and microscopic images

21951071, 0, Downloaded from https://advanced.onlinelibrary.wiley.com/doi/10.1002/adom.72050 by deng pan - University Of Science , Wiley Online Library on [16/11/2026]. See the Terms and Conditions (https://onlinelibrary.wiley.com/terms-and-conditions) on Wiley Online Library for rules of use; OA articles are governed by the applicable Creative Commons License

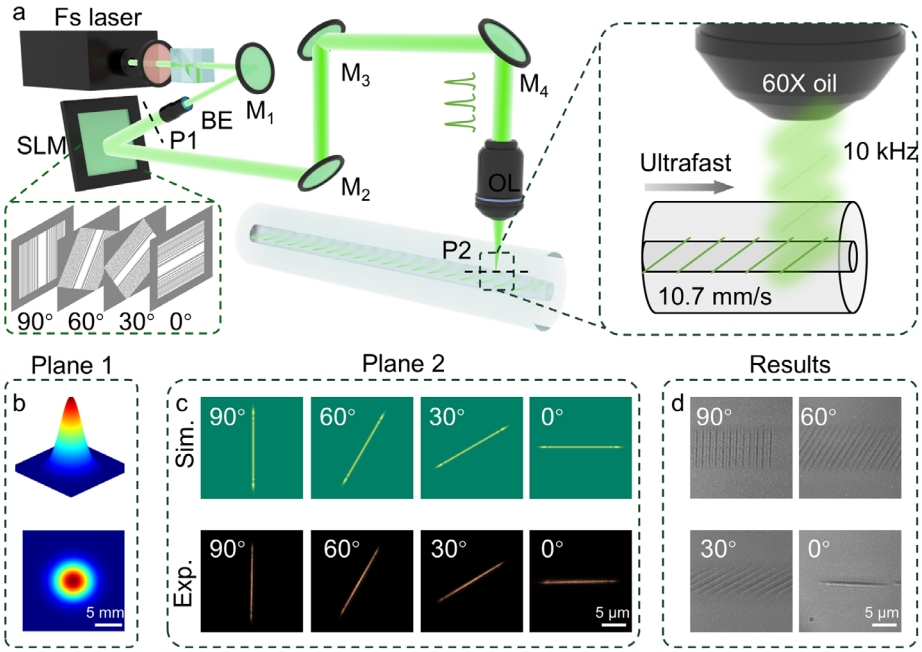

FIGURE 1 | Programmable femtosecond line-focus inscription of TFBGs. (a) Schematic diagram of the experimental setup for TFBG fabrication based on SLM-enabled cylindrical-lens phase modulation of a femtosecond laser. The incident Gaussian beam is wavefront-modulated by the SLM and focused into the fiber core through a high-NA oil-immersion objective to generate a line-shaped focal field. (b) Simulated 3D and transverse intensity distributions of the incident Gaussian beam before line-focus formation. (c) Theoretical and experimental intensity distributions of the line-shaped structured optical field generated by femtosecond laser cylindrical lens beam shaping at $\theta = 0°$, 30°, 60°, and 90°. (d) Optical microscope images of the corresponding laser-inscribed line-shaped modification structures in the fiber core at $\theta = 0°$, 30°, 60°, and 90°.

of the inscribed structures further confirmed that tilted grating planes with different orientations could be reliably formed in the fiber core (Figure 1d). Microscope-based measurements of ten traces at each nominal tilt angle from 0° to 45° in 5° increments yielded an approximately one-to-one relationship between the mean measured and programmed angles: $\theta_{measured} = 1.00046\ \theta_{programmed} + 0.62669°$, with $R^2 = 0.99853$ (Figure S7). The maximum absolute deviation of a group mean was 1.502°, and the trace-to-trace sample standard deviations ranged from 0.214° to 0.962°. The nominal 0° group exhibited a measured angle of 0.842° ± 0.214°. These projected angles were referenced to the direction perpendicular to the fiber-core axis; the measurement procedure is provided in the Supporting Information. Because the grating planes are generated by a line-shaped focal field rather than by serial point-by-point scanning, a typical 6 mm TFBG can be fabricated within 0.56 s at a translation speed of 10.7 mm/s. Further fabrication flexibility is demonstrated by combined 0°/45° trace patterns formed through successive scans and spatially segmented structures with trace orientations of 0°, 15°, 30°, and 45° (Figure S6). These structures were produced by updating the SLM phase hologram without mechanically rotating the shaping element.

2.2 | Spectral Control and Parameter Optimization of Low-Tilt TFBGs

After establishing the programmable line-focus inscription scheme, we investigated how key fabrication parameters determine the spectral response of low-tilt TFBGs. In low-tilt regime, efficient coupling from the forward core mode to backward cladding modes produces a dense set of cladding-mode resonances in the transmission spectrum. The strength, spectral position, and insertion loss of these resonances are governed by the grating length, tilt angle, modulation period, and laser pulse energy. Therefore, systematic optimization of these parameters is essential for obtaining high-quality TFBGs for refractive-index sensing.

We first examined the influence of grating length while keeping the period and pulse energy fixed at 1.07 μm and 1.37 μJ, respectively. As the grating length increased from 2 to 8 mm, the cladding-mode resonance strength increased monotonically from below 7 dB to above 20 dB, accompanied by a gradual increase in insertion loss (Figure 2a). This behavior is consistent with the increased interaction length between the guided core mode and the tilted refractive-index modulation. A grating length of 6 mm was therefore selected as a balanced condition that provides strong cladding-mode resonances while maintaining acceptable insertion loss.

The tilt angle provides another important degree of freedom for spectral engineering. For TFBGs with tilt angles from 0° to 15°, increasing the tilt angle resulted in a clear blue shift of the cladding-mode resonance envelope (Figure 2b). This trend reflects the phase-matching condition for coupling from the core mode to higher-order backward-propagating cladding modes with lower effective refractive indices. The ability to tune the resonance envelope by simply rotating the SLM-loaded phase hologram highlights the flexibility of the proposed method compared with fixed phase-mask-based approaches.

21951071, 0, Downloaded from https://advanced.onlinelibrary.wiley.com/doi/10.1002/adom.72050 by deng pan - University Of Science , Wiley Online Library on [16/11/2026]. See the Terms and Conditions (https://onlinelibrary.wiley.com/terms-and-conditions) on Wiley Online Library for rules of use; OA articles are governed by the applicable Creative Commons License

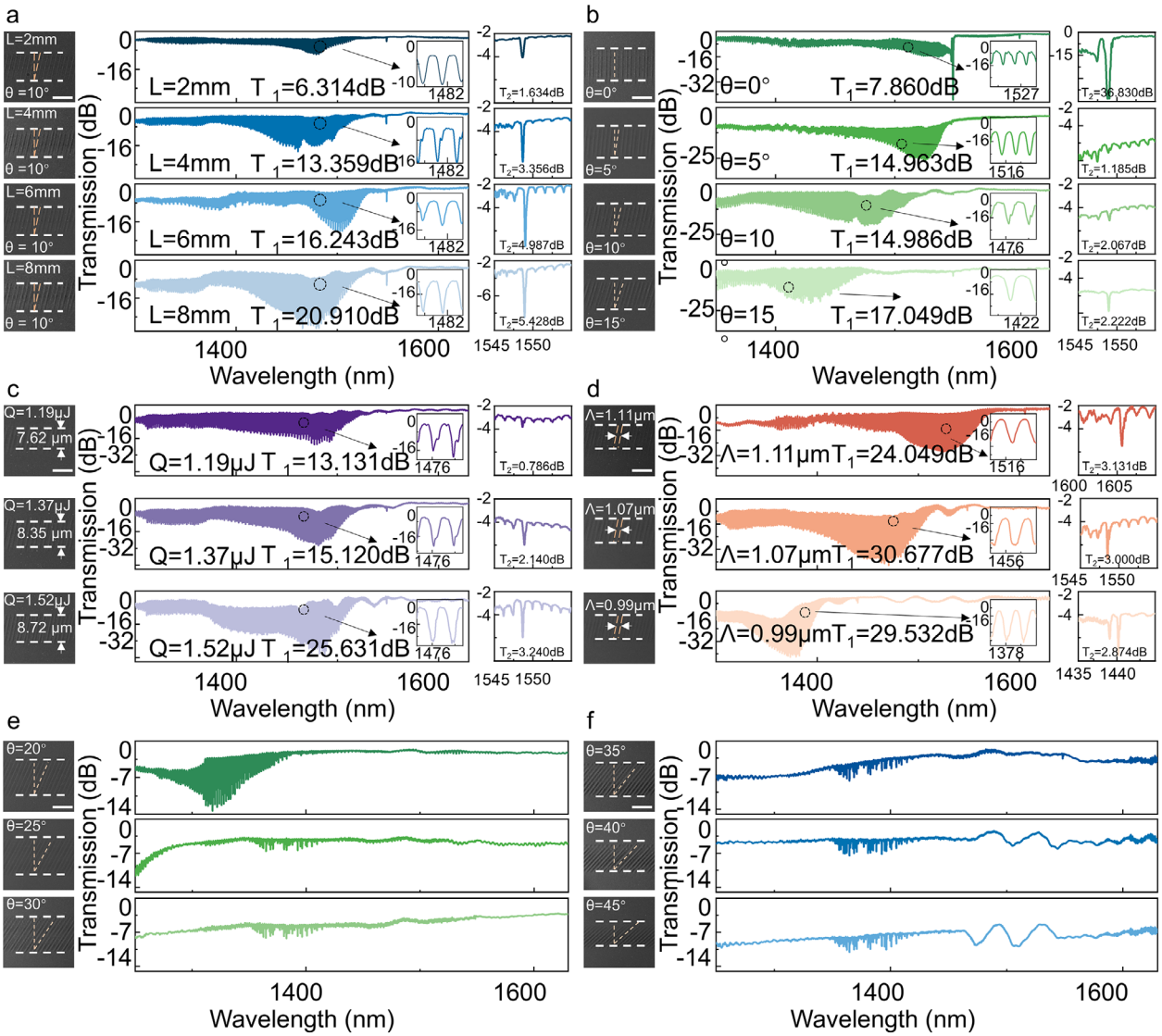

FIGURE 2 | Spectral control of low-tilt TFBGs by programmable femtosecond line-focus inscription. (a) Microscope images and transmission spectra of 10° TFBGs with grating lengths of 2, 4, 6, and 8 mm, fabricated under the same grating period and pulse energy. Increasing the grating length enhances the cladding-mode resonance strength while gradually increasing insertion loss. (b) Microscope images and transmission spectra of TFBGs with tilt angles of 0°, 5°, 10°, and 15°, fabricated with the same grating length, period, and pulse energy. The cladding-mode resonance envelope shifts with increasing tilt angle, reflecting angle-dependent mode coupling. (c) Microscope images and transmission spectra of 10° TFBGs fabricated with pulse energies of 1.19, 1.37, and 1.52 μJ under the same grating length and period. Higher pulse energy strengthens the refractive-index modulation, whereas excessive energy increases insertion loss. (d) Microscope images and transmission spectra of 10° TFBGs with grating periods of 1.11, 1.07, and 0.9941 μm, fabricated under the same pulse energy and grating length. Decreasing the period shifts the cladding-mode resonances toward shorter wavelengths. (e) Transmission spectra of the TFBG with tilt angles of 20°, 25°, 30°, 35°, 40°, and 45° under the optimal process parameters.

Pulse energy was then optimized to control the refractive-index modulation strength. Increasing the pulse energy from 1.19 to 1.52 μJ enhanced the cladding-mode resonance strength from 13.13 to 25.63 dB (Figure 2c). However, increasing the pulse energy from 1.37 to 1.52 μJ resulted in a pronounced increase in insertion loss. Therefore, 1.37 μJ was selected as a processing parameter that balances cladding-mode resonance strength and insertion loss under the tested conditions.

Finally, decreasing the grating period produced a pronounced blue shift of the cladding-mode resonance band, in good agreement with the phase-matching relation (Figure 2d). Based on these results, a tilt angle of 10°, a grating length of 6 mm, a period of 1.07 μm, and a pulse energy of 1.37 μJ were selected as optimized parameters for sensing-oriented low-tilt TFBGs.

Device reproducibility was assessed using three independently fabricated TFBGs at each tilt angle of 10° and 20°. The spectra of the three devices at each angle are compared in Figure S4, with 153 and 69 resonance dips jointly matched across the three 10° and three 20° spectra, respectively. The analysis procedure is provided in the Supporting Information. These results provide preliminary evidence of fabrication repeatability and spectral consistency among the tested devices. Further studies with larger sample sizes can help establish large-scale manufacturing capability. Additional alignment experiments identify core

21951071, 0, Downloaded from https://advanced.onlinelibrary.wiley.com/doi/10.1002/adom.72050 by deng pan - University Of Science , Wiley Online Library on [16/11/2026]. See the Terms and Conditions (https://onlinelibrary.wiley.com/terms-and-conditions) on Wiley Online Library for rules of use; OA articles are governed by the applicable Creative Commons License

positioning and writing-trajectory alignment as factors affecting grating formation (Figure S5).

2.3 | High-Tilt TFBGs Enabled by Programmable Angular Control

Beyond low-tilt gratings for cladding-mode sensing, the programmable angular control of the SLM-based inscription system also enables the fabrication of high-tilt TFBGs. This capability is particularly important because high-tilt gratings operate in a distinct physical regime: instead of producing dense discrete cladding-mode resonances, they increasingly behave as blazed in-fiber structures with strong polarization-dependent coupling. Such polarization-selective transmission is highly desirable for all-fiber polarizing elements and nonlinear-polarization-rotation mode-locked lasers.

TFBGs with tilt angles from 20° to 45° were fabricated using the same line-focus inscription platform with a single-pulse energy of 1.37 μJ and a processing speed of 1.07 mm/s (Figure 2e). At a tilt angle of 20°, pronounced cladding-mode resonances were still observed. As the tilt angle increased to 25° and beyond, the discrete cladding-mode resonances became progressively weaker. This evolution can be understood from two complementary mechanisms [28, 29]. First, the phase-matching condition shifts the coupled modes toward higher-order cladding modes with lower effective refractive indices. When these modes approach the cutoff condition, they become increasingly leaky and eventually transform into radiation-like modes. Second, the coupling becomes more strongly blazed at large tilt angles, causing more optical power to be coupled laterally rather than into discrete backward cladding modes. Therefore, the weakening of cladding-mode resonances at large tilt angles does not indicate a failure of grating fabrication; instead, it marks the transition from a sensing-oriented cladding-mode coupling regime to a polarization-oriented blazed-grating regime.

2.4 | Ultrafast Fabrication and Comparison with Point-by-Point Inscription

A central advantage of the proposed line-focus inscription strategy is its ability to decouple TFBG fabrication from slow and discontinuous point-by-point scanning. In conventional femtosecond point-by-point writing, tilted grating planes are constructed through a sequence of discrete modification points along segmented trajectories. This process requires frequent changes in the stage motion direction or velocity, making the inscription sensitive to stage inertia and speed fluctuations. As a result, increasing the writing speed often leads to degraded structural uniformity and poor spectral quality. In contrast, the line-shaped focal field used in our method directly defines each tilted grating plane, allowing TFBGs to be written through simple continuous translation.

To quantitatively evaluate the fabrication efficiency, we compared the proposed SLM-based line-focus inscription method with conventional femtosecond point-by-point writing under identical grating parameters, including a period of 1.07 μm, a tilt angle of 10°, and a grating length of 6 mm (Figure 3a,b). For point-by-point inscription, acceptable cladding-mode resonances were obtained only at relatively low translation speeds. When the speed was increased beyond 0.25 mm/s, the spectral quality degraded rapidly, with the cladding-mode resonance strength decreasing to 4.7 and 3.4 dB at 0.3 and 0.35 mm/s, respectively. This degradation is attributed to the increased influence of stage inertia and nonuniform motion during segmented-path writing (Figure 3d).

In contrast, the proposed line-focus inscription method maintained stable grating spectra over a broad writing-speed range from 0.107 to 10.7 mm/s. Even at the maximum speed of 10.7 mm/s, the cladding-mode resonance strength remained approximately 30 dB, demonstrating that the line-shaped focal field enables both high-speed and high-fidelity TFBG fabrication (Figure 3c). For a typical 6 mm TFBG, the inscription time was reduced to 0.56 s, representing an improvement of approximately three orders of magnitude compared with conventional point-by-point writing.

The high fabrication speed further enables rapid production of cascaded TFBG arrays. To examine whether high-speed inscription can also be achieved at a large tilt angle, we fabricated 45° TFBGs at translation speeds of 0.107, 1.07, 5.35, and 10.7 mm/s (Figure S8). The grating length was fixed at 6 mm, and the single-pulse energy was kept constant. The effective pulse repetition rates were adjusted to 100, 1, 5, and 10 kHz, respectively, maintaining a nominal axial grating period of 1.07 μm according to $\Lambda_z = v/f_{eff}$. The transmission spectra were measured over 1250–1650 nm under the same polarization conditions.

Pronounced wavelength-dependent spectral features remain evident at all four writing speeds, including attenuation features in the approximately 1490–1545 nm region. At 10.7 mm/s, the nominal scanning time for a 6 mm grating is approximately 0.56 s, excluding positioning, alignment, and other preparation steps. These results support the feasibility of high-speed inscription of 45° TFBGs. However, differences in the overall spectral levels and in the positions and depths of the spectral features remain apparent. The comparison therefore demonstrates retained spectral response at the highest tested speed, without establishing equivalent spectral or polarization performance across writing conditions as a demonstration, 6 mm TFBGs were inscribed sequentially along a single fiber using the same programmable line-focus strategy (Figure 3e). The inset of Figure 3e shows a sample image of eight cascaded 2 mm gratings fabricated on a single optical fiber, with a total fabrication time of only 4.48 s. Notably, the resulting gratings exhibited clearly separated spectral features and stable resonance characteristics (Figure 3f), confirming that the method is suitable not only for individual TFBG devices but also for array-based fiber sensing architectures.

2.5 | Low-Tilt TFBGs for Refractive-Index and Moisture Sensing

The strong cladding-mode resonances of low-tilt TFBGs make them well suited for refractive-index sensing. When broadband light propagates through a TFBG, part of the core-mode energy is coupled into backward-propagating cladding modes. Because the cladding modes interact with the external medium through their evanescent fields, changes in the surrounding refractive index

21951071, 0, Downloaded from https://advanced.onlinelibrary.wiley.com/doi/10.1002/adom.72050 by deng pan - University Of Science , Wiley Online Library on [16/11/2026]. See the Terms and Conditions (https://onlinelibrary.wiley.com/terms-and-conditions) on Wiley Online Library for rules of use; OA articles are governed by the applicable Creative Commons License

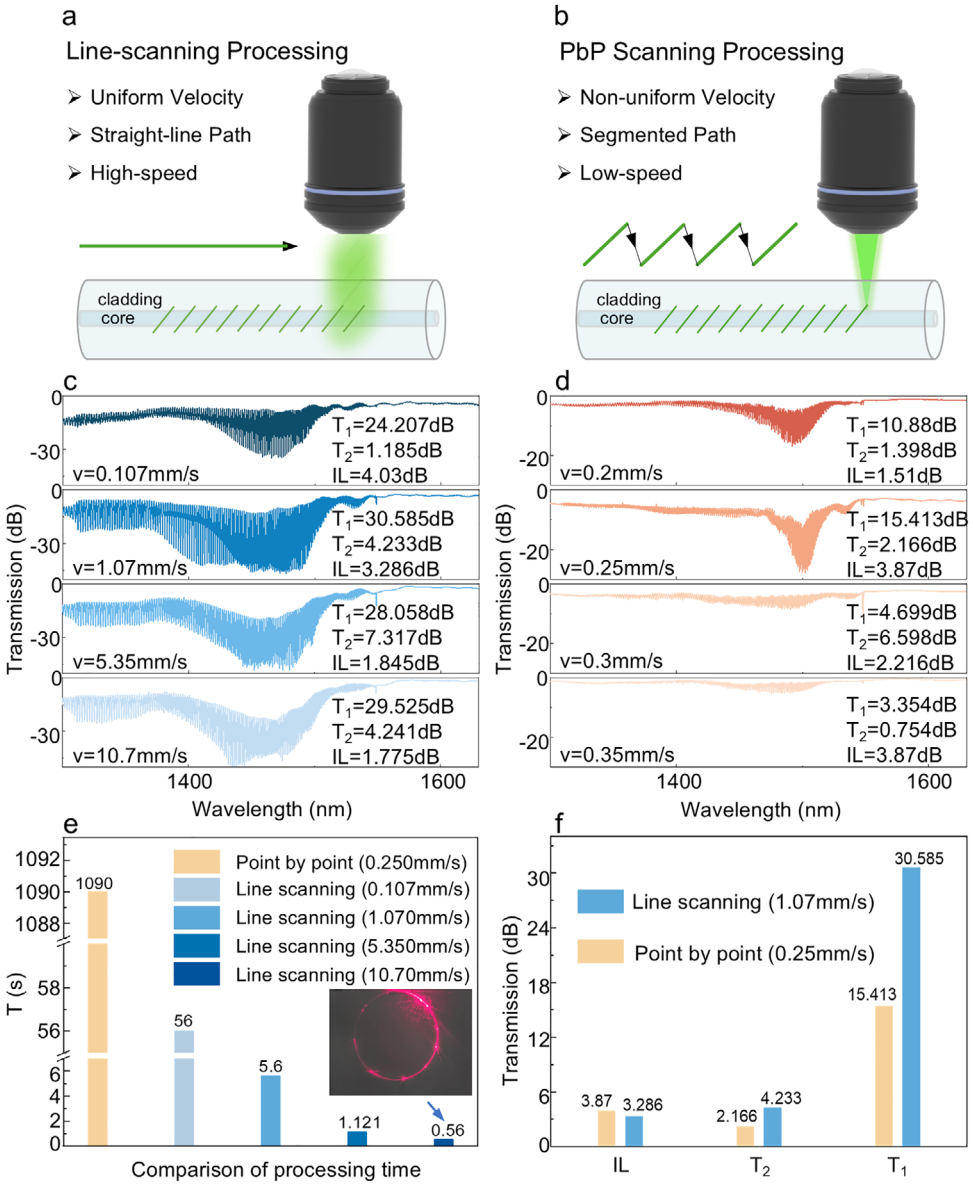

FIGURE 3 | Comparison of TFBGs fabrication efficiency between line-focus inscription and point-by-point writing. (a) Schematic of TFBG inscription using the proposed SLM-based line-focus method. (b) Schematic of conventional femtosecond point-by-point TFBG inscription. (c) Transmission spectra of 10° TFBGs fabricated at different translation speeds using the proposed method. (d) Transmission spectra of 10° TFBGs fabricated at different translation speeds using the point-by-point method. (e) Comparison of fabrication time under optimized conditions. Inset, optical microscope image of eight cascaded TFBGs inscribed on a single fiber using the proposed method. (f) Comparison of the spectral characteristics of TFBGs fabricated by the proposed method at 1.07 mm s^{-1} and by the point-by-point method at 0.25 mm s^{-1}.

modify the modal boundary conditions and lead to measurable variations in the transmission spectrum (Figure 4a). The Bragg resonance associated with the core mode, in contrast, remains largely insensitive to the surrounding medium and can serve as an internal spectral reference.

A 10° TFBG fabricated under the optimized low-tilt conditions was characterized using sucrose solutions with refractive indices ranging from 1.330 to 1.407 (Figure 4b). As the external refractive index increased, the high-order cladding-mode resonances in the short-wavelength region gradually weakened and eventually disappeared when the surrounding refractive index approached the effective refractive index of the corresponding cladding modes. This behavior indicates the transition of guided cladding modes into leaky modes. The cutoff wavelength exhibited a linear dependence on the external refractive index, yielding a sensitivity of 410.7 nm/RIU, while the Bragg wavelength remained nearly unchanged (Figure 4c). These results confirm that the fabricated low-tilt TFBGs can provide high-sensitivity and self-referenced refractive-index sensing.

The ultrafast fabrication capability of the proposed method further allows multiple TFBGs to be cascaded along a single fiber for multi-point sensing. To demonstrate this capability, three 10° TFBGs were inscribed at different positions along the same fiber with spectrally separated operating bands. As shown in Figure 4(d)), a broadband light source illuminates the three cascaded TFBGs, and an optical spectrum analyzer

21951071, 0, Downloaded from https://advanced.onlinelibrary.wiley.com/doi/10.1002/adom.72050 by deng pan - University Of Science , Wiley Online Library on [16/11/2026]. See the Terms and Conditions (https://onlinelibrary.wiley.com/terms-and-conditions) on Wiley Online Library for rules of use; OA articles are governed by the applicable Creative Commons License

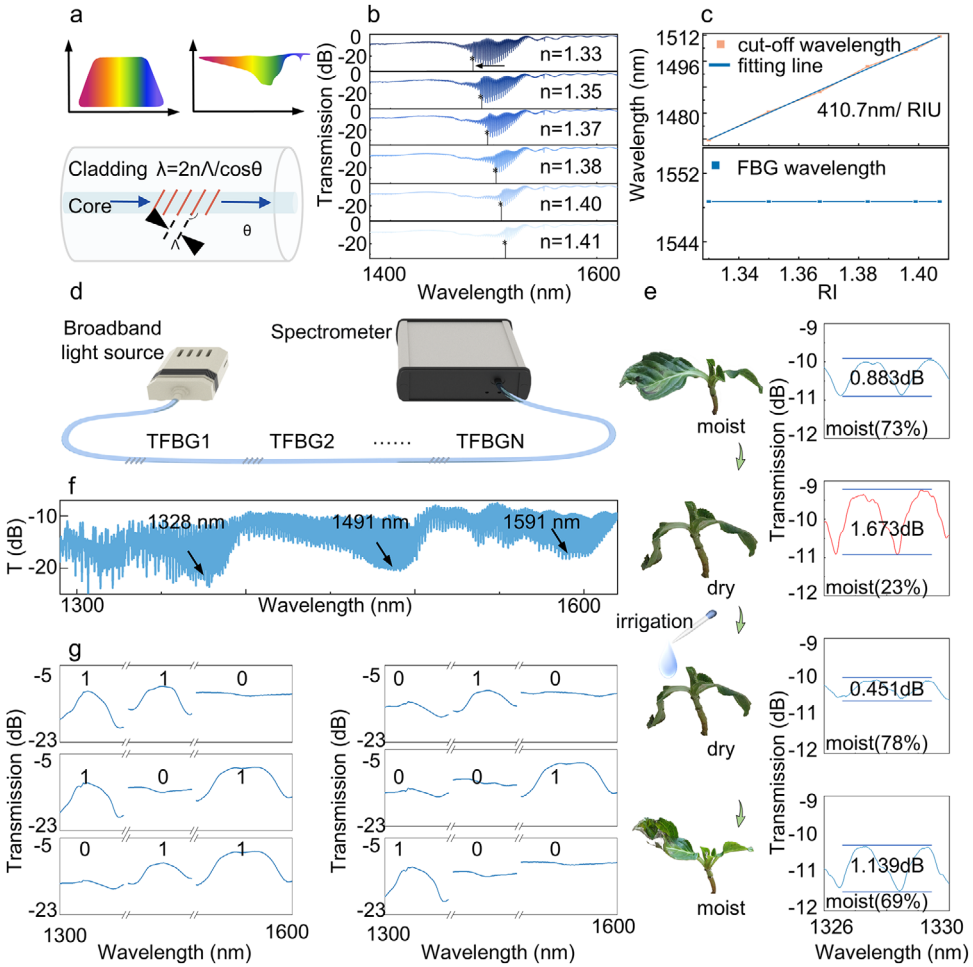

FIGURE 4 | Cascaded low-tilt TFBGs for refractive-index and moisture sensing. (a) Schematic of the refractive-index sensing mechanism of a low-tilt TFBG. (b) Transmission spectra of a 10° TFBG measured in liquids with different refractive indices. (c) Cutoff wavelength and Bragg wavelength shifts as functions of refractive index from 1.330 to 1.407, with linear fits.(d) Schematic of the cascaded TFBG sensing setup, comprising a broadband light source, three cascaded TFBGs, and an optical spectrum analyzer. The arrow indicates the direction of light propagation. (e) Plant growth status and corresponding transmission spectra at soil moisture levels of 73%, 23%, 78%, and 69%. (f) Spectral responses of the three sensing bands in the cascaded low-tilt TFBG sensor under six experimental conditions. (g) Transmission spectra of the three sensing bands under the six experimental conditions.

records their transmission spectrum. Liquid contact at each sensing location is identified from changes in the spectral band associated with the corresponding grating. The transmission spectrum exhibited three distinct resonance envelopes centered at 1328 nm, 1491 nm, and 1591 nm, corresponding to the three sensing locations (Figure 4f). When a specific grating section was exposed to water, the high-order cladding-mode resonances in the corresponding spectral band disappeared, whereas the other bands remained unchanged. This independent spectral response enables a simple binary identification scheme for local liquid contact and confirms the low cross-talk among the cascaded sensing channels (Figure 4g).

As a proof-of-concept application, the cascaded TFBG sensor was used to monitor plant root-zone water status (Figure 4e). The grating sections were buried near the plant roots. Under high soil moisture conditions, the cladding-mode attenuation was strong and the transmission intensity remained low. As the soil became dry, the spectral intensity increased, providing an optical indication of water deficiency near the root zone. After irrigation, the soil moisture recovered and the spectral intensity decreased accordingly. This reversible response demonstrates the potential of cascaded TFBG sensors for real-time root-zone moisture monitoring and precision irrigation.

2.6 | High-Tilt TFBGs for all-Fiber Mode-Locked Lasers

Tilted fiber Bragg gratings have polarization-dependent transmission, owning unique advantages including high polarization extinction ratio (PER), low insertion loss, broadband responsivity, and flexible working wavelength. Due to its polarization-dependent loss and all-fiber structure, TFBGs can be used as effective polarizers to introduce the polarization-dependent loss in the laser cavity. Quantitatively, polarization-dependent loss (PDL) measurements confirm that the PDL increases substantially with tilt angle, reaching ~15 dB for 45° TFBGs across the C-band, thereby providing the polarization selectivity essential for NPR mode-locking (Figure S3). The two polarization

21951071, 0, Downloaded from https://advanced.onlinelibrary.wiley.com/doi/10.1002/adom.72050 by deng pan - University Of Science , Wiley Online Library on [16/11/2026]. See the Terms and Conditions (https://onlinelibrary.wiley.com/terms-and-conditions) on Wiley Online Library for rules of use; OA articles are governed by the applicable Creative Commons License

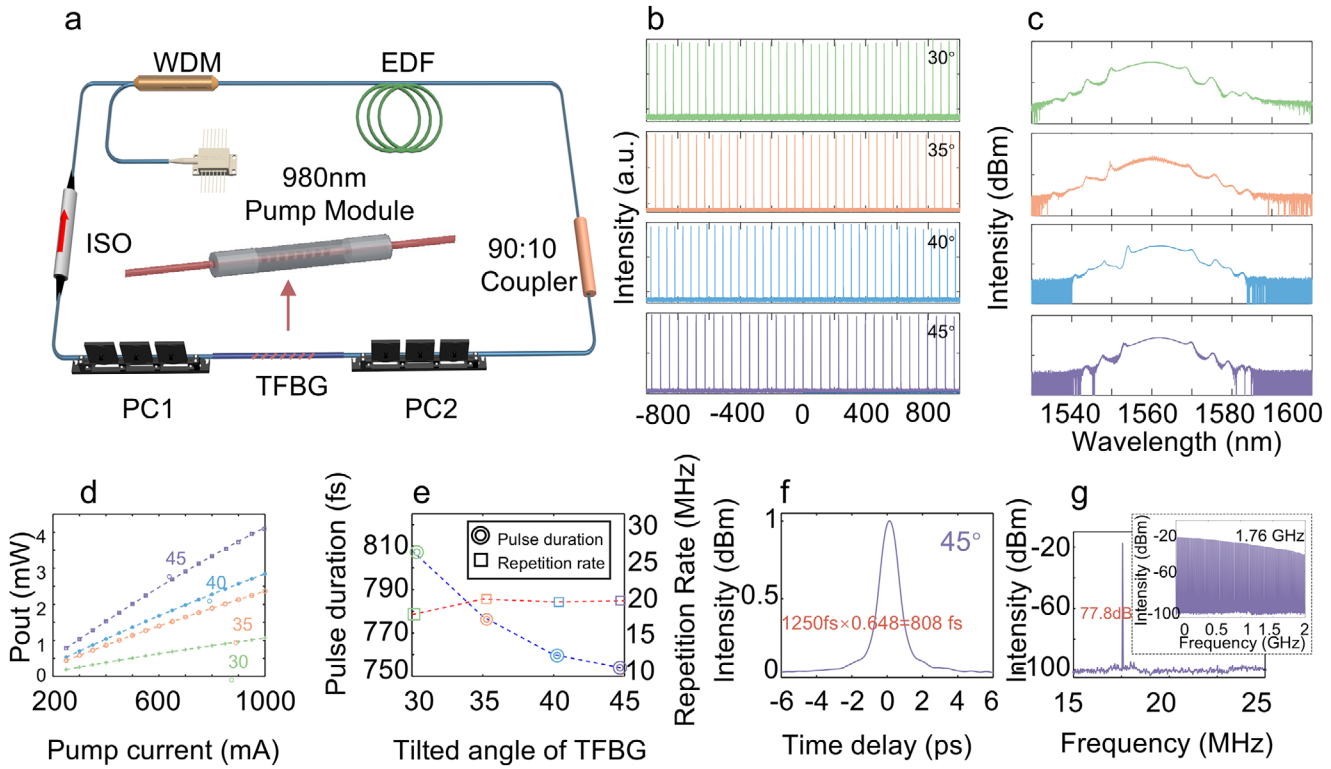

FIGURE 5 | Experimental results of mode-locking based on TFBG with different tilted angles. (a) Experimental setup of mode-locked fiber laser based on tilted fiber Bragg gratings (TFBGs). (b) Pulse trains at 1000 mA. (c) Optical spectra at 1000 mA. (d) Output power as a function of pump current for TFBGs with four different angles. (e) Pulse duration (Left) and Laser repetition rate (Right) as a function of the tilted angle of TFBGs. (f) Autocorrelation trace of mode-locked pulses with a 45° TFBG. And (g) Radiofrequency (RF) spectrum over a narrow range of 1.76 GHz with a resolution of 29 kHz and RF spectrum in a large range of 2 GHz with a resolution of 2.9 MHz.

controllers (PCs) adjust the polarization state launched into the cavity fiber and the returning polarization state relative to the polarization-selective transmission of the TFBG. Together with Kerr-induced nonlinear polarization evolution in the cavity fiber, their adjustment enables intensity-dependent transmission through the TFBG, providing an effective saturable absorber for nonlinear polarization rotation (NPR) mode locking. By showcasing the application of our fabricated TFBGs, we conducted all-fiber mode-locked lasers using fabricated TFBGs with different tilted angles. The experimental setup of the lasers is depicted (Figure 5(a)). In this setup, a piece of 1.41 m Erbium-doped fiber (EDF) is pumped by a 980 nm laser diode with a maximum pump power of 700 mW. A polarization-independent isolator is placed in the laser cavity to guarantee unidirectional operation. For characterization, 10% of the intracavity energy is extracted through a 10:90 optical coupler, while the remaining 90% of light circulates in the laser cavity. Four fabricated TFBGs with different tilted angles are employed in the laser cavity.

The experimental results of the TFBGs-based mode-locking are shown (Figure 5). The stable pulse train mode-locked with 30° TFBG, 35° TFBG, 40° TFBG, and 45° TFBG is depicted from top to bottom (Figure 5(b)). The corresponding spectra are shown from top to bottom (Figure 5(c)). Symmetrical Kelly sidebands are observed, confirming the stable operation of mode-locking. The central wavelengths in these four cases are in the C band determined by the gain range of EDF, while subtle differences in the central wavelength are caused by the slight difference in the center wavelength of the fabricated TFBGs. The output power as a function of the pump current is demonstrated (Figure 5(d)), exhibiting clear thresholds for mode-locking and linear relationships between the pump current and the output power. For TFBG with a small angle, for instance, a 30° TFBG, the slope, namely the output laser efficiency of the laser is low. This may be due to the low PER when compared with TFBG with large titled angles. The highest laser efficiency is achieved when a 45° TFBG is used. We would like to emphasize here that our scope aims to demonstrate the successful application of our fabricated TFBG with different angles in ultrafast lasers. Optimization of the laser performances in terms of the laser efficiency, spectral width, as well as pulse duration, and pulse energy, can be further enhanced by engineering the laser cavity dispersion and laser configuration. The pulse duration (Left) and the fundamental pulse repetition rate (Right) of mode-locked pulses are shown (Figure 5(e)). The repetition rates of the laser for four different TFBGs are almost the same, at a value of nearly 1.76 GHz, as only TFBGs are replaced in the laser cavity. The minor change in the repetition rate is due to the different lengths of the pigtails of TFBGs. It is worth noting that the pulse durations for different TFBGs are all in the sub-picosecond regime, suggesting our fabricated TFBGs are cost-effective in the generation of ultrashort pulses. The autocorrelation trace of mode-locked pulses with a 45° TFBG yields a pulse duration of 808 fs (Figure 5(f)). The corresponding radio frequency spectrum over a range of 1.76 GHz with a resolution of 29 kHz achieves a high signal-to-noise ratio of

21951071, 0, Downloaded from https://advanced.onlinelibrary.wiley.com/doi/10.1002/adom.72050 by deng pan - University Of Science , Wiley Online Library on [16/11/2026]. See the Terms and Conditions (https://onlinelibrary.wiley.com/terms-and-conditions) on Wiley Online Library for rules of use; OA articles are governed by the applicable Creative Commons License

77.8 dB (Figure 5(g)). The RF spectrum over a wide range of 2 GHz confirms the high quality of stable mode-locking operation.

3 | Discussion

Here, the proposed method offers the advantages of high fabrication efficiency and programmable structural control. Compared with point-focus scanning-based approaches, the focal line directly defines each trace, reducing transverse scanning and return motion. Slit simulations clarify the dependence of transmission on aperture dimensions (Figure S1), while experiments demonstrate approximately fourfold higher useful optical power utilization for SLM-based shaping than for the tested slit configuration (Figure S2). Additional measurements establish the polarization selectivity of high-tilt gratings (Figure S3), support device spectral consistency (Figure S4), and identify positioning and alignment conditions for further improving fabrication stability (Figure S5). Updating the SLM phase hologram enables focal-line rotation, combined-orientation patterns, and spatially segmented structures without mechanically rotating the shaping element (Figure S6). This simplified writing strategy maintains strong cladding-mode resonances in the tested 10° TFBGs at speeds up to 10.7 mm/s and retains characteristic transmission features in 45° TFBGs at the same speed (Figure S8), enabling a nominal fabrication time of 0.56 s for a 6 mm grating and rapid fabrication of cascaded arrays for multi-point sensing.

In summary, we have demonstrated an SLM-enabled femtosecond line-focus inscription strategy for ultrafast and angle-programmable fabrication of tilted fiber Bragg gratings. By loading a cylindrical-lens phase hologram onto the SLM, a high-aspect-ratio femtosecond focal field was generated inside the fiber core, and its orientation could be controlled by rotating the phase hologram. This programmable wavefront-shaping approach enables TFBGs with tilt angles from 0° to 45° to be fabricated without replacing phase masks or optical components. Two representative applications were demonstrated to highlight the versatility of the platform. Low-tilt TFBGs achieved refractive-index sensing with a sensitivity of 410.7 nm/RIU and were further applied to cascaded moisture sensing and plant root-zone water-status monitoring. High-tilt TFBGs were integrated into erbium-doped fiber laser cavities as polarization-dependent components for nonlinear-polarization-rotation mode locking, producing stable sub-picosecond pulses with a pulse duration of 808 fs and an RF signal-to-noise ratio of 77.8 dB. These results show that SLM-based femtosecond line-focus inscription provides a flexible, efficient, and scalable route to application-specific TFBGs, with promising potential in distributed fiber sensing, polarization-selective photonics, and ultrafast fiber lasers

4 | Methods

4.1 | Fabrication of TFBGs

The processing procedure for the optical fiber sample is as follows: first, the coating is stripped from the fiber, and the bare fiber is cleaned with anhydrous ethanol to ensure a clean and intact surface. The fiber is then fixed onto a glass slide with auxiliary alignment markings, and the slide is placed on the sample holder of a high-precision 3D translation stage.

A commercial femtosecond laser processing system (Monaco, wavelength 517 nm, pulse duration 290 fs, repetition rate 200 kHz) is used for grating fabrication. The laser beam first passes through a zero-order half-wave plate and a Glan–Taylor prism to adjust the pulse energy. After collimation and beam expansion, it is incident upon a spatial light modulator (SLM), which loads a rotatable cylindrical lens phase hologram to modulate the phase of the incident beam. The modulated beam is then focused onto the core region of the prepared single-mode fiber through an oil-immersion objective lens (UPlanSApo 60×/1.35 Oil ∞/0.17/FN26.5). By moving the fiber continuously along a single direction, each femtosecond pulse generates a line-shaped optical field within the fiber core, thereby inscribing the grating structure point by point. The tilt angle of the grating is controlled by rotating the cylindrical lens phase pattern on the SLM. Key fabrication parameters such as grating length, period, tilt angle, and pulse energy are systematically varied to optimize grating performance. Typical fabrication conditions are as follows: grating length 6 mm, period 1.07 μm, tilt angle 10°, pulse energy 1.37 μJ. The translation speed during fabrication is adjusted in the range of 0.107 mm/s to 10.7 mm/s according to experimental requirements.

4.2 | Characterization of TFBGs

The transmission spectra of the fabricated tilted fiber Bragg gratings (TFBGs) are measured using a high-resolution optical spectrum analyzer with a resolution of 0.02 nm over the wavelength range of 1300–1650 nm. A broadband light source is coupled into the fiber, and the transmitted light is collected for spectral analysis. The cladding mode resonance strength, insertion loss, and spectral envelope shift are evaluated as functions of key fabrication parameters, including the grating tilt angle, length, period, and pulse energy. For refractive index sensing experiments, the TFBG is immersed in standard sucrose solutions with refractive indices ranging from 1.33 to 1.407, and the corresponding spectral responses are recorded.

4.3 | Mode-Locked Laser Setup

The fabricated tilted fiber Bragg gratings (TFBGs) are integrated into an all-fiber mode-locked laser cavity to evaluate their polarization-dependent loss characteristics. The laser cavity consists of a 1.41 m erbium-doped fiber and a 980 nm laser diode with a maximum pump power of 700 mW. A polarization-independent isolator is incorporated into the cavity to ensure unidirectional operation. A 10:90 optical coupler is used to extract 10% of the intracavity energy for output characterization, while the remaining 90% of the light circulates within the cavity. Two polarization controllers are placed in the cavity to facilitate the mode-locking mechanism based on nonlinear polarization rotation. TFBGs with different tilt angles (30°, 35°, 40°, and 45°) are individually inserted into the cavity, and the mode-locking performance is characterized in terms of output power, pulse duration, repetition rate, and radio-frequency spectrum.

21951071, 0, Downloaded from https://advanced.onlinelibrary.wiley.com/doi/10.1002/adom.72050 by deng pan - University Of Science , Wiley Online Library on [16/11/2026]. See the Terms and Conditions (https://onlinelibrary.wiley.com/terms-and-conditions) on Wiley Online Library for rules of use; OA articles are governed by the applicable Creative Commons License

Author Contributions

Deng Pan: conceptualization, methodology, visualization, writing – original draft, review and editing. **Yihang Yin**: investigation, writing – original draft. **Hai Hu**: investigation, writing – original draft. **Zhijuan Fuyang**: investigation, writing – original draft. **Chenchu Zhang**: supervision, methodology, writing – review and editing. **Hui Wang**: formal analysis. **Shenglai Zhen**: supervision, writing – review and editing. **Yanlei Hu**: formal analysis, validation. **Jiawen Li**: formal analysis, data curation. **Zhaoxin Lao**: supervision, data curation. **Zhiqiang Wang**: validation, supervision, writing – review and editing. **Benli Yu**: writing – review and editing, supervision. **Dong Wu**: conceptualization, methodology, writing – review and editing.

Acknowledgements

This work was supported by the National Key Research and Development Program of China (2024YFB4610700), the National Natural Science Foundation of China (Nos. 62325507, 52375582, 62205236, 62461160305, 62475066), Scientific Research Project of Anhui Provincial Department of Education (2025AHGXZK20171, 2024AH050067), the Fundamental Research Funds for the Central Universities of China (Grant Number. PA2025IISL0103). We acknowledge the Modern Experiment Technology Center of Anhui University and Experimental Center of Engineering and the Material Sciences at USTC for their support in sample fabrication and characterization. This work was partially carried out at the USTC Center for Micro and Nanoscale Research and Fabrication and Instruments Center for Physical Science, University of Science and Technology of China. The analysis work of this article was partially carried out at the Instrumental Analysis Center, Hefei University of Technology.

Funding

National Key Research and Development Program of China (2024YFB4610700); National Natural Science Foundation of China (Nos. 62325507, 52375582, 62205236, 62461160305, 62475066); Scientific Research Project of Anhui Provincial Department of Education (2025AHGXZK20171, 2024AH050067); Fundamental Research Funds for the Central Universities of China (PA2025IISL0103).

Conflicts of Interest

The authors declare no conflicts of interest.

Data Availability Statement

The data that support the findings of this study are available from the corresponding author upon reasonable request.

References

1. W. Li, Y. Long, Y. Yan, et al., "Wearable Photonic Smart Wristband for Cardiorespiratory Function Assessment and Biometric Identification," *Opto-Electronic Advances* 8, no. 5, (2025): 240254, https://doi.org/10.29026/oea.2025.240254.

2. G. Meltz, W. W. Morey, and G. W. Glenn, *In Optical Fiber Communication Conference* (Optical Society of America, 1990).

3. T. Erdogan and J. E. Sipe, "Tilted fiber Phase Gratings," *Journal of the Optical Society of America A* 13, no. 2, (1996): 296–313, https://doi.org/10.1364/JOSAA.13.000296.

4. R. Wang, H. Zhang, Q. Liu, et al., "Operando Monitoring of Ion Activities in Aqueous Batteries With Plasmonic fiber-optic Sensors," *Nature Communications* 13, no. 1, (2022): 547, https://doi.org/10.1038/s41467-022-28267-y.

5. X. Han, H. Zhong, K. Li, et al., "Operando Monitoring of Dendrite Formation in Lithium Metal Batteries via Ultrasensitive Tilted fiber Bragg Grating Sensors," *Light: Science & Applications* 13, no. 1, (2024): 24, https://doi.org/10.1038/s41377-023-01346-5.

6. J. Lao, P. Sun, F. Liu, et al., "In Situ Plasmonic Optical fiber Detection of the state of Charge of Supercapacitors for Renewable Energy Storage," *Light: Science & Applications* 7, no. 1, (2018): 34, https://doi.org/10.1038/s41377-018-0040-y.

7. F. Liu, W. Lu, J. Huang, et al., "Detangling Electrolyte Chemical Dynamics in Lithium Sulfur Batteries by Operando Monitoring With Optical Resonance Combs," *Nature Communications* 14, no. 1, (2023): 7350, https://doi.org/10.1038/s41467-023-43110-8.

8. L. Liu, X. Zhang, Q. Zhu, et al., "Ultrasensitive Detection of Endocrine Disruptors via Superfine Plasmonic Spectral Combs," *Light: Science & Applications* 10, no. 1, (2021): 181, https://doi.org/10.1038/s41377-021-00618-2.

9. K. Zhou, G. Simpson, X. Chen, L. Zhang, and I. Bennion, "High Extinction Ratio in-fiber Polarizers Based on 45° Tilted fiber Bragg Gratings," *Optics Letters* 30, no. 11, (2005): 1285–1287, https://doi.org/10.1364/OL.30.001285.

10. C. Caucheteur, T. Guo, F. Liu, B. O. Guan, and J. Albert, "Ultrasensitive Plasmonic Sensing in Air Using Optical Fibre Spectral Combs," *Nature Communications* 7, no. 1, (2016): 13371, https://doi.org/10.1038/ncomms13371.

11. R. Suo, X. Chen, K. Zhou, L. Zhang, and I. Bennion, "In-fibre Directional Transverse Loading Sensor Based on Excessively Tilted Fibre Bragg Gratings," *Measurement Science and Technology* 20, no. 3, (2009): 034015, https://doi.org/10.1088/0957-0233/20/3/034015.

12. L. Liu, F. Chen, X. Xiao, et al., "Direct femtosecond laser inscription of an IR fluorotellurite fiber Bragg grating," *Optics Letters* 46, no. 19, (2021): 4832, https://doi.org/10.1364/OL.439290.

13. S. Yang, Q. Zhang, L. Yang, et al., "Optomechanical Sensor Network With fiber Bragg Gratings," *Nature Communications* 16, no. 1, (2025): 10795, https://doi.org/10.1038/s41467-025-66350-2.

14. Y. Tao, W. Xu, P. Yu, et al., "Programmable Direct-patterning Assembly Enables High-density and Surface-conformal Integration of fiber Bragg Grating Sensor Arrays," *Nature Communications* 17, no. 1, (2026): 5998, https://doi.org/10.1038/s41467-026-72613-3.

15. K. Zhou, A. G. Simpson, L. Zhang, and I. Bennion, "Side Detection of Strong Radiation-mode Out-coupling From Blazed FBGs in Single-mode and Multimode Fibers," *IEEE Photonics Technology Letters* 15, no. 7, (2003): 936–938, https://doi.org/10.1109/LPT.2003.813568.

16. N. S. Yazd, K. Chah, C. Caucheteur, and P. Megret, "Thermal Regeneration of Tilted Bragg Gratings UV Photo-inscribed in Hydrogen-loaded Standard Optical Fibers," *Journal of Lightwave Technology* 39, no. 11, (2021): 3582–3590, https://doi.org/10.1109/JLT.2021.3066676.

17. K. O. Hill, B. Malo, F. Bilodeau, D. C. Johnson, and J. Albert, "Bragg Gratings Fabricated in Monomode Photosensitive Optical fiber by UV Exposure Through a Phase Mask," *Applied Physics Letters* 62, no. 10, (1993): 1035–1037, https://doi.org/10.1063/1.108786.

18. S. J. Mihailov, R. B. Walker, T. J. Stocki, and D. C. Johnson, "Fabrication of a Tilted fiber-grating Polarization-dependent Loss equalizer," in *Bragg Gratings, Photosensitivity, and Poling in Glass Waveguides* (Optical Society of America, 2001), https://doi.org/10.1364/BGPP.2001.BFD2.

19. R. Wang, J. Si, T. Chen, et al., "Fabrication of High-temperature Tilted fiber Bragg Gratings Using a Femtosecond Laser," *Optics Express* 25, no. 20, (2017): 23684–23689, https://doi.org/10.1364/OE.25.023684.

20. X. Li, W. Bao, F. Chen, A. Yang, R. Wang, and X. Qiao, "High Temperature Sustainable Tilted fiber Bragg Gratings via Femtosecond Laser Plane-by-plane Writing Technology," *Journal of Lightwave Technology* 41, no. 13, (2023): 4290–4296, https://doi.org/10.1109/JLT.2022.3218853.

21. P. Roldan-Varona, D. Pallares-Aldeiturriaga, L. Rodriguez-Cobo, and J. M. Lopez-Higuera, "Slit Beam Shaping Technique for Femtosecond Laser Inscription of Enhanced Plane-by-plane FBGs," *Journal of Lightwave Technology* 38, no. 16, (2020): 4526–4532, https://doi.org/10.1109/JLT.2020.2992568.

21951071, 0, Downloaded from https://advanced.onlinelibrary.wiley.com/doi/10.1002/adom.72050 by deng pan - University Of Science , Wiley Online Library on [16/11/2026]. See the Terms and Conditions (https://onlinelibrary.wiley.com/terms-and-conditions) on Wiley Online Library for rules of use; OA articles are governed by the applicable Creative Commons License

22. Y. Tan, et al., "Femtosecond Laser Three-dimensional Isotropic Inscription in Glass Enabled by High-speed Rotating Slit Beam Shaping," *Int J Extrem Manuf* 8 (2025): 015001, https://doi.org/10.1088/2631-7990/ae0539.

23. D. Strickland and G. Mourou, "Compression of Amplified Chirped Optical Pulses," *Optics Communications* 56, no. 3, (1985): 219–221, https://doi.org/10.1016/0030-4018(85)90120-8.

24. Y. Lai, K. Zhou, K. Sugden, and I. Bennion, "Point-by-point Inscription of First-order fiber Bragg Grating for C-band Applications," *Optics Express* 15, no. 26, (2007): 18318–18325, https://doi.org/10.1364/OE.15.018318.

25. D. Pan, Z. Fuyang, H. Wang, et al., "Designed 3D Dumpling-Shaped Femtosecond Laser Structured Light Field for Nanoscale Sensing," *Advanced Functional Materials* 34, no. 37, (2024): 2402323, https://doi.org/10.1002/adfm.202402323.

26. J. W. Goodman, *Introduction to Fourier Optics* (McGraw-Hill, 1968).

27. C. Rosales-Guzmán and A. Forbes, *How to Shape Light With Spatial Light Modulators* (SPIE Press, 2017), https://doi.org/10.1117/3.2281295.

28. J. Albert, L.-Y. Shao, and C. Caucheteur, "Tilted fiber Bragg Grating Sensors," *Laser & Photonics Reviews* 7, no. 1, (2013): 83–108, https://doi.org/10.1002/lpor.201100039.

29. K. Zhou, L. Zhang, X. Chen, and I. Bennion, "Low Thermal Sensitivity Grating Devices Based on Ex-45° Tilting Structure Capable of Forward-Propagating Cladding Modes Coupling," *Journal of Lightwave Technology* 24, no. 12, (2006): 5087–5094, https://doi.org/10.1109/JLT.2006.884985.

Supporting Information

Additional supporting information can be found online in the Supporting Information section.

Supporting File: adom72050-sup-0001-SuppMat.docx.

21951071, 0, Downloaded from https://advanced.onlinelibrary.wiley.com/doi/10.1002/adom.72050 by deng pan - University Of Science , Wiley Online Library on [16/11/2026]. See the Terms and Conditions (https://onlinelibrary.wiley.com/terms-and-conditions) on Wiley Online Library for rules of use; OA articles are governed by the applicable Creative Commons License